Journal of Manufacturing Processes 32 (2018) 664–675

Contents lists available at ScienceDirect

Journal of Manufacturing Processes

journal homepage: www.elsevier.com/locate/manpro

Ultrasonic Additive Manufacturing as a form-then-bond process for embedding electronic circuitry into a metal matrix

Alkaios Bournias-Varotsis[a,*], Ross J. Friel[b], Russell A. Harris[c], Daniel S. Engstrøm[a,*]

[a] Wolfson School of Mechanical, Electrical and Manufacturing Engineering, Loughborough University, Loughborough LE11 3TU, United Kingdom
[b] MAX IV Laboratory, Lund University, P.O. Box 118, SE-221 00 Lund, Sweden
[c] Mechanical Engineering, The University of Leeds, Leeds LS2 9JT, United Kingdom

ARTICLE INFO

Keywords:
Additive manufacturing
3D printing
Embedded electronics
Ultrasonic Additive Manufacturing
Ultrasonic consolidation
Plastic deformation

ABSTRACT

Ultrasonic Additive Manufacturing (UAM) is a hybrid manufacturing process that involves the layer-by-layer ultrasonic welding of metal foils in the solid state with periodic CNC machining to achieve the desired 3D shape. UAM enables the fabrication of metal smart structures, because it allows the embedding of various components into the metal matrix, due to the high degree of plastic metal flow and the relatively low temperatures encountered during the layer bonding process. To further the embedding capabilities of UAM, in this paper we examine the ultrasonic welding of aluminium foils with features machined prior to bonding. These pre-machined features can be stacked layer-by-layer to create pockets for the accommodation of fragile components, such as electronic circuitry, prior to encapsulation. This manufacturing approach transforms UAM into a "form-then-bond" process. By studying the deformation of aluminium foils during UAM, a statistical model was developed that allowed the prediction of the final location, dimensions and tolerances of pre-machined features for a set of UAM process parameters. The predictive power of the model was demonstrated by designing a cavity to accommodate an electronic component (i.e. a surface mount resistor) prior to its encapsulation within the metal matrix. We also further emphasised the importance of the tensioning force in the UAM process. The current work paves the way for the creation of a novel system for the fabrication of three-dimensional electronic circuits embedded into an additively manufactured complex metal composite.

1. Introduction

Ultrasonic Additive Manufacturing (UAM) is a hybrid sheet lamination/Computer Numerical Control (CNC) manufacturing process. UAM utilizes Ultrasonic Welding (UW) to bond thin metal foils in a layer-by-layer fashion and periodic CNC machining to create the desired 3D shape. The technology was first introduced by White [1] under the name of Ultrasonic Consolidation. During the bonding step, a cylindrical textured machine tool, called the sonotrode, is pressed at a constant normal force against the metal foil, which is kept in place via a clamping or tensioning mechanism. The sonotrode rolls over the foil while oscillating at a constant frequency of approx. 20 kHz perpendicular to the direction of travel (see Fig. 1). This results in the creation of a solid state bond between the interfaces of the foil and the metallic substrate. The process is then repeated until the desired height is reached.

The quality of bonding during UAM depends on multiple processing and material parameters, however, the three main process parameters are the sonotrode's amplitude of oscillation [μm], the sonotrode exerted normal force [N], and the linear speed [mm/s] of the sonotrode. The effect of each of these processing parameters was closely examined for the first time by Kong et al. [2], who identified that an optimum set exists past which degradation of the previously formed bonds occurs. More recent studies by Hopkins et al. [3] and Wolcott et al. [4] identified the amplitude and weld speed as the most significant parameters for creating high-quality bonds in UAM of aluminium alloys.

Bonding in UAM occurs at a relatively low temperature. This was measured by Kelly et al. [5] using an infrared camera and higher amplitudes of oscillation (> 25 μm) and Schick et al. [6] and Sriraman et al. [7] by embedding thermocouples in the foil-foil interface at lower amplitudes (< 25 μm). All three studies reported a peak temperature considerably lower than the melting point of aluminium (under 250 °C in the first case and less than 100 °C in the later cases) that dissipates rapidly away from the bonding interface. Moreover, a relatively high degree of plastic metal flow is induced during ultrasonic bonding, which has been studied extensively by Kong et al. [8] and Yang et al.

* Corresponding authors.
E-mail addresses: A.Bournias-Varotsis@lboro.ac.uk (A. Bournias-Varotsis), Ross.Friel@maxiv.lu.se (R.J. Friel), R.Harris@leeds.ac.uk (R.A. Harris), D.Engstrom@lboro.ac.uk (D.S. Engstrøm).

https://doi.org/10.1016/j.jmapro.2018.03.027
Received 1 June 2017; Received in revised form 20 March 2018; Accepted 22 March 2018

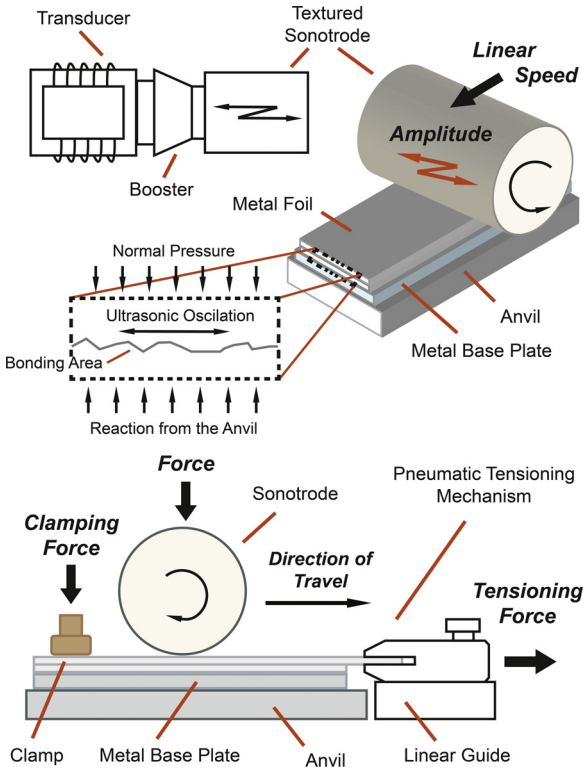

Fig. 1. Schematic overview of Ultrasonic Additive Manufacturing (UAM).

[9] using different machine setups. Both researchers concluded that an increase in the amplitude of oscillations promotes the plastic metal flow due to mechanisms, such as the acoustic softening phenomenon.

These unique properties of UAM have been exploited in the past allowing the embedding of various electronic structures into a metal matrix. For example, Li et al. [10] reported the embedding of printed electronic pathways directly between the aluminium foil interfaces and Siggard et al. [11] and Robinson et al. [12] encapsulated pre-packed electronic circuitry and printed electronic pathways respectively in CNC machined substrate pockets. Moreover, metal matrix composites have been successfully manufactured using UAM. For example, Kong and Soar [13] have successfully embedded polymer-coated and uncoated optical fibres in an aluminium matrix, while similar work has been carried out by Monaghan et al. [14] and Mou et al. [15] for embedding metal-coated optical fibres and Bragg fibres respectively. Shape memory alloy fibres have been embedded in aluminium using UAM by Friel and Harris [16] and Hahnlen and Dapino [17] fabricated an active metal matrix composite in a similar fashion using NiTi fibres. In each of the aforementioned studies, the researchers reported good functionality of the embedded components and very good bond strength in the welded interfaces of the metal foils and thus UAM is considered an enabler for the fabrication of smart metal structures.

After UAM bonding several layers, a CNC machining step is introduced to give the desired form to the bonded metal foils. The cycle of bonding metal foils onto the previously fabricated and formed part and machining the newly bonded layers to shape is repeated until the part is complete. For this reason, Gibson et al. [18] categorised UAM as a "bond-then-form" process in their review of the sheet lamination technologies.

An alternative methodology for creating 3D objects through a sheet lamination process is the "form-then-bond" approach [18]. In this approach, the desired shape is given to each layer (e.g. via razor cutting, or laser machining) prior to bonding it to the previously fabricated part. This enables the creation of structures with internal features and channels, which are more difficult to manufacture with a bond-then-form methodology. The benefits of this approach have been demonstrated by Cawley et al. [19], who successfully manufactured functional ceramic components and microfluidic devices using the Computer-Aided Manufacturing of Laminated Engineering Materials (CAM-LEM) method, and by Thabourey et al. [20], who developed a methodology for the manufacturing of die casting moulds with internal cooling channels.

UAM has previously been shown capable of embedding electronic components such as sensors and antennas as shown by Siggard et al. [11] and Robinson et al. [12] respectively. Moreover, 2D printed electronic pathways were embedded directly between the foil-foil interfaces by Li et al. [10]. However, new more compact electronic designs rely on a 3D architecture with vertical vias connecting each layer electrically. Traditional UAM requires milling or drilling to connect subsequent layers, which can risk damaging underlying electronic components. Moreover, metal chips and lubricant can create short circuits. On the other hand, the form-then-bond method allows for prefabricated vias with no need for further post-processing. A form-then-bond approach would also enable the preparation or pre-treatment (chemical, mechanical or other) of the metal foils prior to bonding. For example, the planar surfaces of aluminium foils and the vertical inner walls of machined features on these foils could be selectively anodized prior to bonding. This way an electrically insulating layer is created onto which planar and vertical electronic interconnects can be deposited and then embedded in creating 3D electronic circuits. This method was examined in a previous article by the author [21], demonstrating its feasibility and limitations, as well as the effect of the ultrasonic power on the resistivity of printed conductive materials [37]. Alternatively, printed electronic interconnects and other electronic circuits (e.g. RFID antennae) could be deposited or attached to the surface of an aluminium foil prior to UAM, which could then be bonded onto a metal substrate, encapsulating the circuit. These novel approaches could provide greater manufacturing capabilities for embedding electronics into a metal matrix and produce components that have direct applications into growing industries, such as the Internet of Things.

By taking advantage of the benefits of the form-then-bond approach, the authors have envisioned an alteration to the traditional UAM manufacturing process, which is illustrated schematically in Fig. 2. In

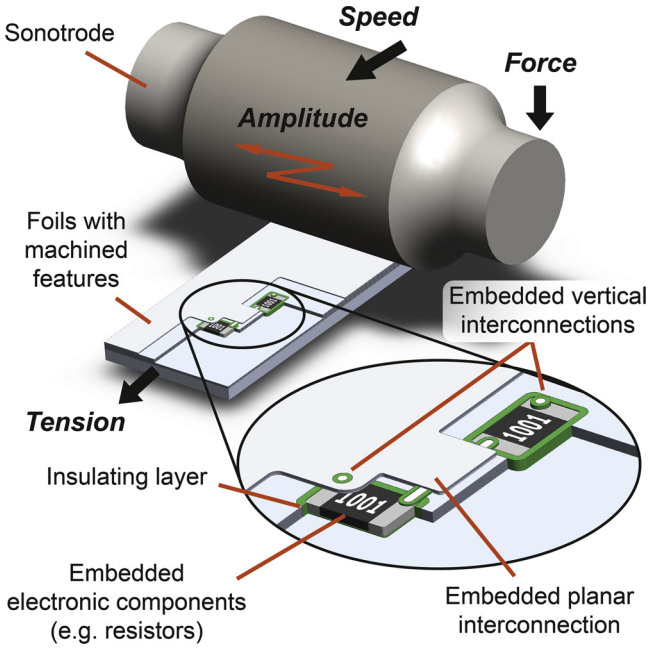

Fig. 2. Illustration of electronic circuitry embedded in a metal matrix using the proposed approach.

this example, we focus on the embedding of electronics, but the same approach could be applied to other fields, such as the fabrication of microfluidic or thermal management devices. In the proposed process, aluminium foils are first machined (using e.g. milling, razor or water-jet cutting or punching) and then bonded using UAM. The pre-machined features are stacked layer-by-layer to create cavities and channels to accommodate pre-packaged electronic circuitry or printed electronic interconnects. The foils can also be altered prior to bonding using any of the methods mentioned in the previous paragraph. The process of manufacturing the external contour of the part, as well as the layers below and above the embedded circuitry, remain the same as in traditional UAM. This method can be advantageous compared to previous attempts to embed electronics using UAM due to the possibility of prefabricating electronic circuits onto the surface metal foil prior to bonding/embedding and the relative flexibility of creating 3-dimensional electronics, with vertical interconnects. Also, this method can facilitate the miniaturization of the embedded structures, resulting in the improved mechanical performance of the manufactured metal part. Miniaturization in this case is beneficial in two ways. Firstly, the embedded structures act as stress concentrators in the metal matrix. The effect of the size and position of the inserts in the overall mechanical performance of the part was studied by Dumstorff et al. [22], who concluded that technologies that allow minimal invasive embedding are to be preferred. Secondly, weld recovery over substrates of reduced stiffness or voids is a common phenomenon in UAM which was reported by Robinson et al. [12] and studied in depth by Swank and Stucker [23]. Reducing the dimensions of the footprint of the embedded electronic structures reduces the total partially supported area and therefore promotes the creation of high quality bonds.

The main challenge to be overcome in order for UAM to be used with the form-then-bond approach is the prediction of the final dimensions and location of the machined feature after welding (see Fig. 3). This is not a trivial task since the elongation of the foil in the direction of welding during the bonding step is relatively large (several mm for every 100 mm of welding). Moreover, UAM is considered by its users as a stochastic process: several parameters are involved in the process that is very difficult to model or control (e.g. the roughness of the sonotrode's texture which is transferred onto the foil during ultrasonic welding). For this reason, the main goal of this study was to evaluate the compatibility of UAM with the form-then-bond approach in terms of predictability and repeatability and to assess the resulting locational and dimensional tolerances of the manufactured cavities.

In this paper we describe the process followed to create a statistical regression model for the prediction of the displacement, elongation and associated tolerances of pre-machined features on aluminium foils for a certain set of UAM processing parameters. We also demonstrate the predictive power of such a model by creating a cavity for the encapsulation of a standard surface mount resistor into the metal matrix, paving the way for future research on using UAM as a form-then-bond process. The results presented in this investigation should be considered as a proof of concept of this alternative method and as a guide for future development of the capabilities of UAM.

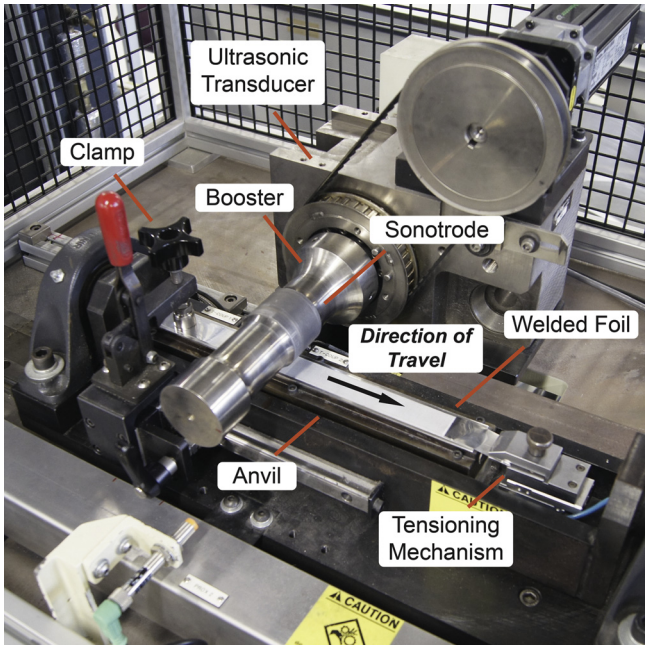

Fig. 4. The Alpha 2 UAM machine.

2. Methods & materials

In this work, the Alpha 2 UAM machine was used (see Fig. 4). This is an experimental setup that allows open access to the machine area, which is ideal for research purposes and has been used for numerous studies in the past [10,14]. It consists of the ultrasonic welder (sonotrode), the anvil, a manual clamp and a pneumatic mechanism for the

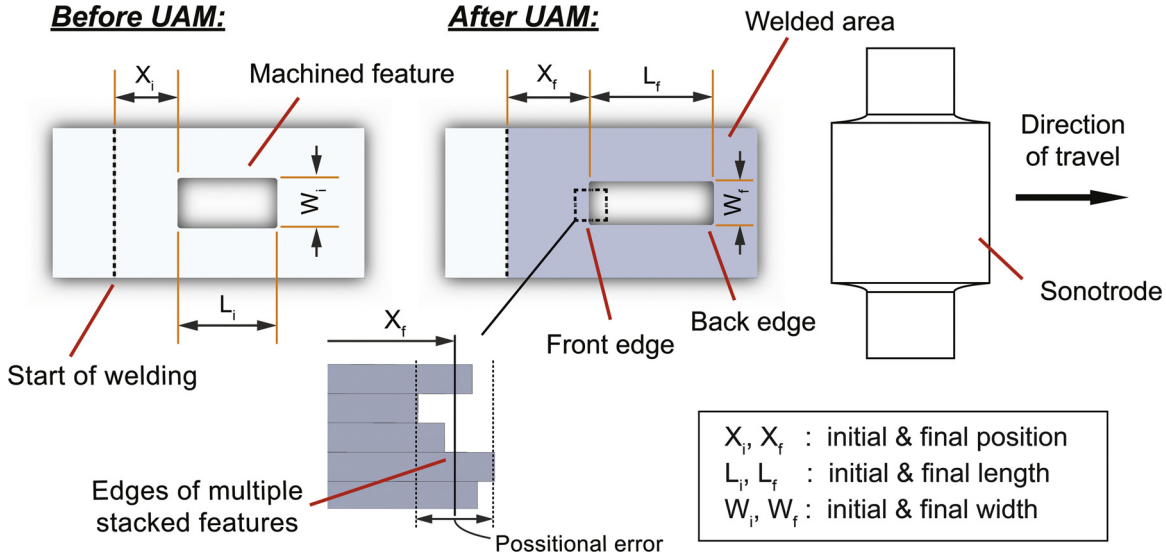

Fig. 3. Deformation of metal foils with machined features during UAM.

tensioning of the foil. The tension mechanism (MXS6-20 guided cylinder, SMC Pneumatics) applies a constant force to the foil and can travel in the direction of welding to compensate for the foil's deformation (the maximum length of travel is approx. 10 mm). The parameters used in this study are within the usual UAM processing parameters and were assessed for their suitability through extensive preliminary experimentation: 18 µm for the amplitude of oscillation, 1600 N for the normal force, 30 mm/s for the linear speed (see Fig. 1). If it is not otherwise specified, a force of 32 N was used for tensioning the foil, as past researchers have determined that this level of the tensioning is sufficient to keep the foil in place during welding. In all experimentation, 100 µm thick and 24 mm wide aluminium Al 3003-H18 foils were used. To prepare the substrates, 2 foils were welded onto a 1.5 mm thick aluminium Al 1050-H14 base plate.

The experimental data collection was organised into three stages to simplify the analysis. In the first stage, the elongation of foils without any machined features was studied and modelled as a function of the initial position from the start of welding. In the second and third stages, rectangular shaped slots were machined onto the aluminium foils prior to welding at a set distance from the start and their displacement and deformation were recorded. In the second stage, only the length of these pre-machined features was varied, while in the third stage the width and length were varied, in order to investigate further the role of the initial dimensions of the pre-machined features to their deformation. These three experimental stages are summarised graphically in Fig. 5.

To study the elongation of foils without any pre-machined features, aluminium foils were marked at regular intervals. A precision blade was used to engrave the foils prior to welding at predetermined nominal locations (i.e. $X_{i,nom}$ = [0, 5, 10, 12.5, 15, 17.5, 20, 25, 35, 45, 55, 65, 75, 85, 95, 105] mm). These marks were straight lines along the whole width of the foil. Their actual initial position (X_i) was verified using an optical Coordinate Measuring Machine (CMM) (SmartScope Flash 200, Optical Gaging Products Inc., NY). The CMM system is annually calibrated and certified to have an accuracy in the XY plane better or equal to $E_{XY} = 2.0 + 6{\cdot}L/1000$ µm where L is in mm. This means that the CMM system provided measurements with an accuracy of better than 3 µm (the maximum distance between features in all three stages was less than 150 mm). The origin of the coordinate system was defined by using as reference the first mark (for the X-axis) and the top edge of the foil (for the Y-axis). For the bonding step, the sonotrode was first placed carefully on the reference mark (start of welding) and then the ultrasonic welding was initiated. The final position of the marks (X_f) was measured with the CMM system and their displacement was calculated (as in $\Delta X = X_f - X_i$). A sufficient number of foils was treated and measured this way to ensure statistically significant results (9 samples, plus 3 extra validation runs). The samples were left overnight in a temperature controlled environment of 20 °C before any measurements were taken.

In order to gain a deeper understanding of the behaviour of the Alpha 2 UAM machine in the area close to the start of welding, a number of samples were cross-sectioned and examined under the optical microscope. The Linear Welding Density (LWD) – defined by Kong et al. [24] as the fraction of the ultrasonically welded length over the total length of the cross-section- of three samples sectioned along their length was measured on intervals of 1 mm and compared with the LWD of a reference sample (3 cross-sections at distance greater than 40 mm from the start of welding).

For the preparation of the foils of the second and third experimental stages, manual milling with a ⌀1 mm diameter cutting tool was used (Europa Milltech 2000VS, spindle speed 2800 rpm, feed speed < 2 cm/min, with coolant). Rectangular slots were machined along the centre axis of a stack of five manually clamped foils simultaneously. Lines were engraved on the foils at a distance of 25 mm from the front edge of the pre-machined features. This mark was used for the placement of the sonotrode during bonding and as a reference for the measurements. The location and surface straightness [25] of each edge of the features were recorded prior and after bonding using the CMM system. Using the collected data the displacement, lengthwise and widthwise deformation of the features were calculated (as in $\Delta X = X_f - X_i$, $\Delta L = L_f - L_i$ and $\Delta W = W_f - W_i$ respectively). In Fig. 6, a typical sample measured with the CMM system and the native Measure-X software after welding is presented. In the same figure, the traced edge is shown and the roughness of the surface of the foil and the edge of the feature due to the textured sonotrode is visible. The automatic line recognition tools of the Measure-X software were used to trace each edge (the software does not specify exactly which algorithms are used).

The width of the features machined onto the aluminium foils for this experimental stage was kept constant at 4.8 mm (or 20% of the width of

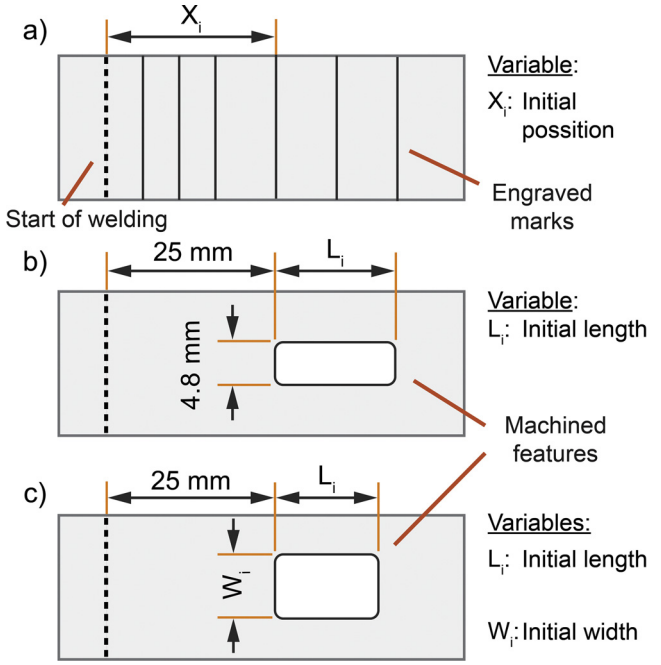

Fig. 5. Schematic of foils used in the (a) first, (b) second and (c) third experimental stages.

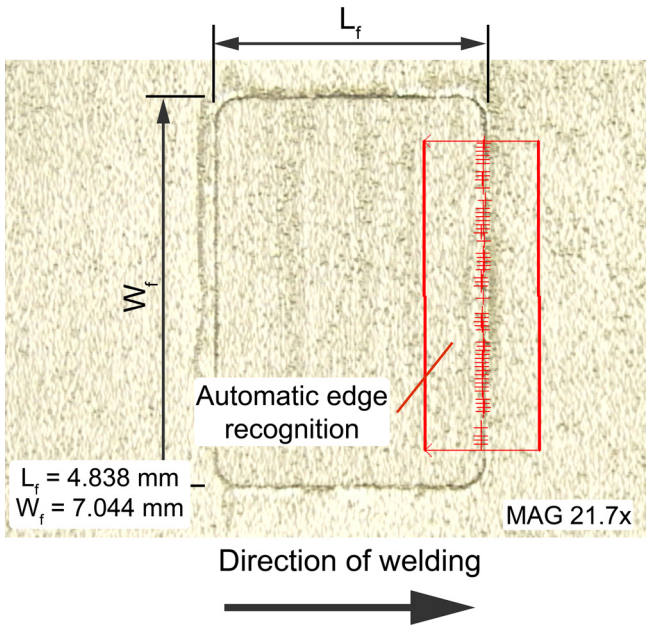

Fig. 6. Typical sample measured with the Coordinate Measuring Machine (CMM).

the foil), while their length was varied from 2.4 mm to 40.8 mm (i.e. $L_{i,nom}$ = [2.4, 7.2, 12.0, 16.8, 21.6, 26.4, 31.2, 36.0, 40.8] mm). By including such a broad range of measurements a deeper understanding of the process was gained. Three foils were prepared and treated for each length.

In the third experimental stage, the effect of the initial dimensions was examined more closely for lengths up to 16.8 mm. In addition, three levels were used for the width of the features (i.e. $W_{i,nom}$ = [2.4, 4.8, 7.2] mm which corresponds to 10%, 20% and 30% of the width of the foil). Preliminary experimentation showed that features with a width larger than 30% of the width of the foil deform very unpredictably during welding, due to the high percentage of missing material, and thus were avoided in this study. A response surface was created using a Doehler D-1 hexagonal design of experiments [26]. Ferreira at al. [27] argued that this experimental design is preferred over other more common designs when the use of different resolutions for the two parameters is desired (e.g. 3 levels for the width and 7 for the length in this case) and because it can be easily expanded by displacing the design towards a promising region, while preserving the runs that had already been performed The nominal initial dimensions of the samples used in this stage are presented in Table 1. Three repetitions were performed for each of the design points. The CMM system was used to verify the actual dimensions of each sample.

The collected data from the three experimental stages were analysed in Matlab. Linear regression models were fitted to each dataset. These models were then combined into a single predictive model, the validity of which was assessed in two instances. First, the displacement and deformation of pre-machined single layer foils were measured and compared to the predicted values. Then a multilayer structure with an embedded electrical component (i.e. a standard TE Connectivity CRG1206 series surface mount resistors with dimensions of 3.10 × 1.65 × 0.55 mm) was fabricated as an example for using the form-then-bond methodology.

3. Results & discussion

3.1. Stage 1: the elongation of foils without machined features

In the first experimental stage, the elongation of aluminium foils with no machined features was assessed. This was accomplished by measuring with the CMM system the location of thin marks created by a precision blade on the top surface of the foils before (X_i) and after (X_f) UAM bonding and calculating their displacement (as in $\Delta X = X_f - X_i$). The marks were measured to be approx. 45 μm wide and 18 μm deep (Talysurf CLI 2000 surface profiling system, Taylor Hobson Ltd). Even though these marks would act as stress raisers, their presence was deemed to have an insignificant effect on the resulting deformation, because (i) the concentration of stresses has a localised effect, [28] and (ii) the intense acoustic softening phenomenon through the volume of the material results in a very high degree of plastic metal flow [8].

The collected experimental data are presented in Fig. 7. In the same figure, the deformation of a foil that was processed at the same levels of force and speed (F = 1600 N, S = 30 mm/s) but with zero amplitude (A = 0) is shown. A comparison between the collected data from the ultrasonically welded samples and the roll-only sample shows that the deformation is greatly amplified by the presence of the ultrasonic

Table 1
Experimental points used in the third (3rd) experimental stage.

Design points	1	2	3	4	5	6	7	8	9	10
Nominal initial length ($L_{i,nom}$) [mm]	2.4	4.8	4.8	7.2	9.6	9.6	12	14.4	14.4	16.8
Nominal initial width ($W_{i,nom}$) [mm]	4.8	2.4	7.2	4.8	2.4	7.2	4.8	2.4	7.2	4.8

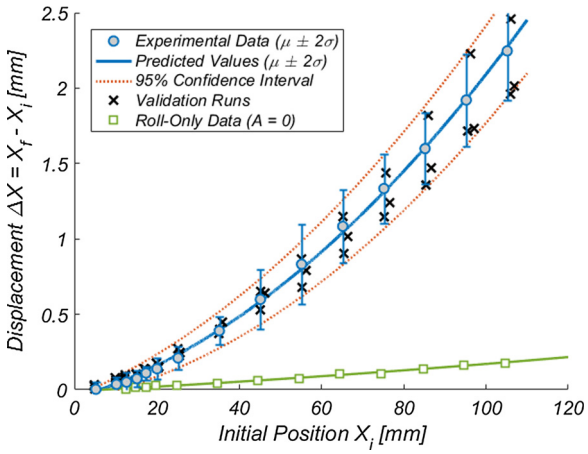

Fig. 7. Experimentally determined deformation of aluminium foils during UAM.

oscillations. In all figures of this study, the error bars represent two times the standard deviation of the collected experimental data (2σ).

A 2nd order linear regression model was fitted to the experimental data (see Appendix, Eq. (A.1). This model was used to predict the mean elongation of the aluminium foils. A 1st order linear model was fitted to the standard deviations of the collected data points (see Appendix Eq. (A.2). This model was used to define the 95% confidence interval for estimating the positional tolerances. Three extra experimental runs were executed for the validation of this model. Both models and the validation runs are presented in Fig. 7. There was a very good agreement between the fitted model and the experimental data (R^2 = 0.99). This is evident in the results of the validation runs, which lay well within the 95% confidence intervals.

The positional error, expressed as the span of the 95% confidence interval, increases linearly with the increase of the initial position (X_i) (from approx. 0.140 mm for X_i = 20 mm to 0.629 mm for X_i = 100 mm). This increase cannot be attributed to a measurement error since average straightness of the marks was approx. 0.050 mm and independent of their initial position. A possible explanation involves the accumulation of angular errors [29]. Due to the design of the tensioning mechanism of the UAM system the precise placement of the foil in the desired location and its alignment with the previous layers is difficult. Moreover, due to the large forces encountered during processing, it is possible that the unbonded foil is slightly displaced during welding in the direction of the ultrasonic oscillations (i.e. perpendicular to the direction of travel). These misalignments can cause angular errors, which are enhanced with distance. Nevertheless, the machine setup was intentionally kept unaltered, in order to evaluate the limitations of the current equipment and provide guidance for future improvements.

It is common knowledge among the users of the Alpha 2 UAM machine that the system has a transitional response at the area near the start of welding. This can be confirmed visually by examining the top surface of the welded foil (see Fig. 8a), as a relationship between the quality of bond and the surface topology of the produced samples has been identified in the past [30,31]: both research articles provided evidence that connects the presence of areas of unaltered texture with inferior quality bonds. This occurs due to a characteristic behaviour of the Alpha 2 UAM machine that is hard-coded into its controller: the sonotrode begins its linear motion before the amplitude of oscillation reaches the value that is set by the user. In order to quantify the length of the transitional area for the set of UAM parameters used in this study, three samples were cross-sectioned lengthwise and their LWD was compared to a reference sample. The results of this measurement are summarised in Fig. 8b. Although the correlation between LWD and the bond strength has been criticised in the past [32], in this study the

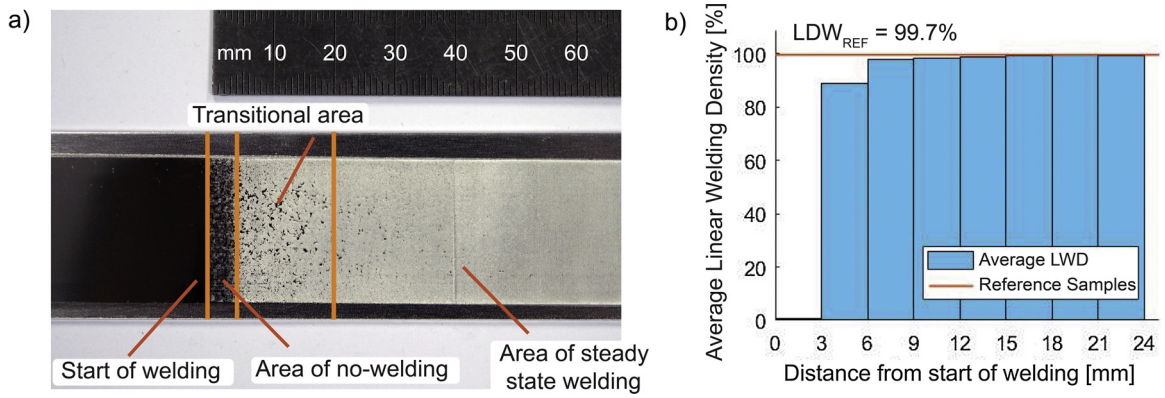

Fig. 8. (a) Photograph of the top surface of a UAM bonded foil and (b) lengthwise LWD measurements close to the start of welding.

lengthwise LWD measurements were used only as an indicator to estimate the distance from the start of welding, after which steady-state ultrasonic welding occurs. It was found that the LWD increases with the distance until it reaches the LWD of the reference sample at approx. 20 mm from the start of welding. This is in accordance with the information gathered through the visual inspection of the samples. For this reason, the pre-machined features used in later stages of this study were placed at a distance of at least 25 mm from the start of welding (i.e. well within the area of steady-state welding).

A key point that has to be made about the experimental results of this section, as well as the results presented throughout this study, is that a particular set of UAM processing parameters (i.e. amplitude, force, speed and temperature) and metals foils with particular characteristics (i.e. material, thickness and width) were examined. The purpose of this investigation was to examine the feasibility of using UAM with the form-then-bond approach and act as a proof-of-concept. The intent of the imposed restrictions was to reduce the number of variables in order to gain a deeper understanding of the process and its limitations. It is expected that the increase of the total energy input (e.g. by increasing the amplitude of oscillations) will result in larger deformation of the metal foil, as was observed during preliminary testing. Moreover, using foils with different material properties or dimensions will result in a different distribution of internal stresses and is expected to have an impact on the observed deformation. Nevertheless, in both the above cases the elongation of the foil during processing is anticipated to follow a similar trend to the that observed in this section response since the underlying governing physical mechanism remains the same.

3.2. Stage 2: the deformation of pre-machined features with variable length & the effect of the tensioning force

In the second experimental stage, the displacement of the edges of rectangular pre-machined features along the direction of travel was examined. Slots of various lengths (from 2.4 mm to 40.8 mm) and constant width (4.8 mm or 20% of the width of the foil) were machined along the centre axis of the foils prior to bonding. By measuring the displacement of the front and back edge of these features (see Fig. 2), a model to predict their final position and length was created. For all runs, the initial nominal position of the front edge of the feature was kept constant at 25 mm, which is inside the steady-state welding area, as determined in the previous section.

The collected data are presented in Fig. 9. Similarly to Section 3.1, a 2nd order linear regression model was fitted to the collected data that was used to predict the mean displacement of the edges (see Appendix Eq. (A.3), and a 1st order linear model was used for the estimation of the 95% confidence interval (see Appendix Eq. (A.4). It was deemed correct to use the displacement data of both the front and back edges for the generation of these models since the displacement of the front

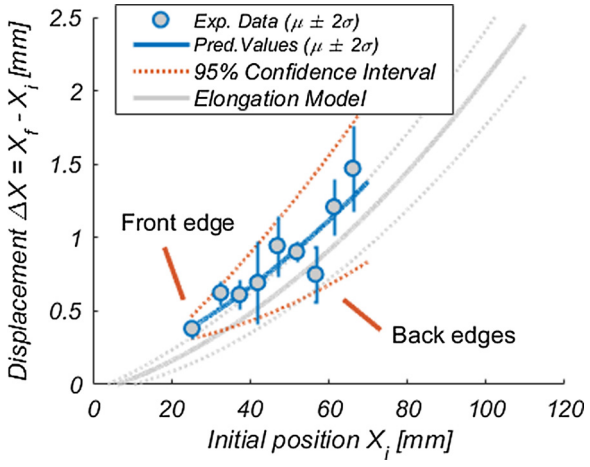

Fig. 9. Experimentally determined deformation of the front and back edges of rectangular features machined onto Al foils prior to bonding.

edge can be interpreted as the displacement of a feature with a length that tends to zero. For comparison, the model generated in Section 3.1 (elongation model) is also plotted in the same figure. A single point falls outside the 95% confidence interval, but there was no experimental reason for this and it was simply considered to be part of the statistical 5% of experiments that will not fall within the 95% confidence interval.

Even though the displacement of the edges of the pre-machined features follows a similar trend to the deformation of the unaltered foil (i.e. 2nd order polynomial for the mean and 1st order for the deviation), there are some important differences. Firstly, the positional error increases at an increased rate. The uncertainty was enhanced due to the presence of the pre-machined features, which lower the stiffness of the foil and adds an additional degree of freedom to the system: in this case, the material can also flow towards the interior of the feature. Secondly, the mean displacement of both front and back edges is significantly higher than the values predicted by the elongation model of Section 3.1. This raised awareness for the importance of the tensioning force, a parameter that has rarely been studied in the past and was not initially included in the model.

A constant tensioning force is applied to the foil during UAM by a pneumatic tensioning mechanism (see Figs. 1 & Figure 4). Previous researchers using the Alpha 2 UAM machine have determined empirically that a suitable value for the tensioning force for Al 3003-H18 foils is approx. 32 N. Lower tensioning force produces suboptimal results because it is not sufficient to keep the foil in place during welding. However, by decreasing the cross-sectional area of the foil by 20% and keeping the force constant, the average equivalent internal tension that is applied to the remaining material is increased by 25% (stress concentration factors were not taken into account, as they have a small

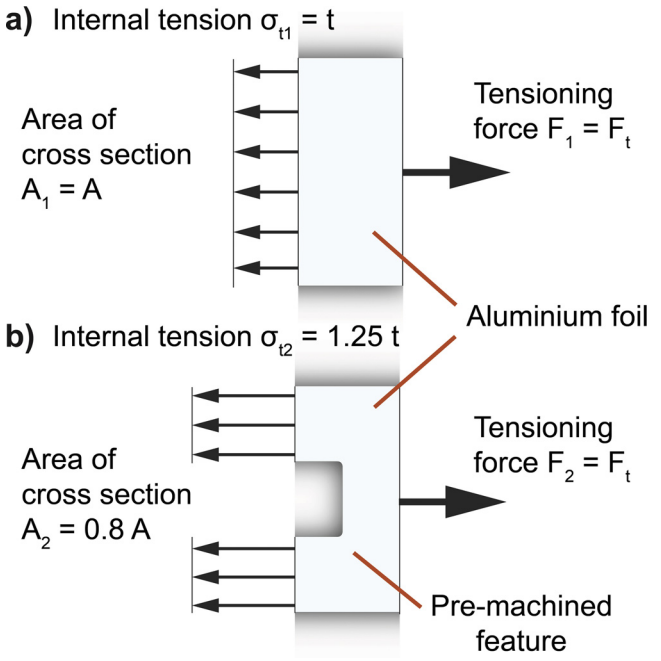

Fig. 10. Schematic representation of the increased internal tension at the presence of a pre-machined feature.

effect in the process, since they decay exponentially from the peak value [28]. This is illustrated in Fig. 10. From past work on the modelling of the rolling process [33], it is known that an increase in the tensioning force (and by extension the internal stresses in the material) decreases the normal force required to achieve a target thickness reduction. In this case, the normal force is kept constant, thus it is expected that the reduction of the thickness of the foils will be increased. The width of the foils before and after UAM bonding was measured using the Talysurf CLI 2000 surface profiling system (3 samples, 10 profiles each) and its increase was negligible (approx. 1%). From the conservation of mass, it was expected that an increased thickness reduction would cause an increase in the elongation of the foil in the longitudinal direction. Thus it was hypothesised that foils with pre-machined features will behave equivalently to foils without any features that were welded using a higher tensioning force.

To further understand the effect of tensioning force on the elongation of the foils during UAM, additional experimental points were collected and added to the dataset of Section 3.1 to create an enhanced model. Foils were prepared in an identical way as in the previous section and were welded onto a substrate using the highest force the tensioning mechanism could produce (i.e. tensioning force $F_{t,high} = 40$ N). Nine (9) samples were prepared this way and the new data points were added to the original dataset of the samples treated at a lower force (i.e. $F_{t,low} = 32$ N). A 2nd order linear regression model was fitted to the means of the new dataset and a 1st order linear model to the standard deviations (see Appendix Eqs. (A.4) and (A.5). A linear relationship was assumed between the tensioning force and the predicted displacement, as only two levels of this parameter were available. In Fig. 11, the collected data and the predictive model are plotted for the low and high levels of the tensioning force. The positional errors did not change significantly between the different levels of the tensioning force, and they were not added to the graph for simplicity.

As anticipated, the elongation of the foils during UAM increased with the application of a higher tensioning force. Moreover, the mean displacement of the edges of pre-machined features with a width equal to 20% of the width of the foil was in good agreement with the deformation of foils welded using 25% higher tensioning force (i.e. $F_t = 40$ N), as it was predicted by the theoretical analysis. Interestingly,

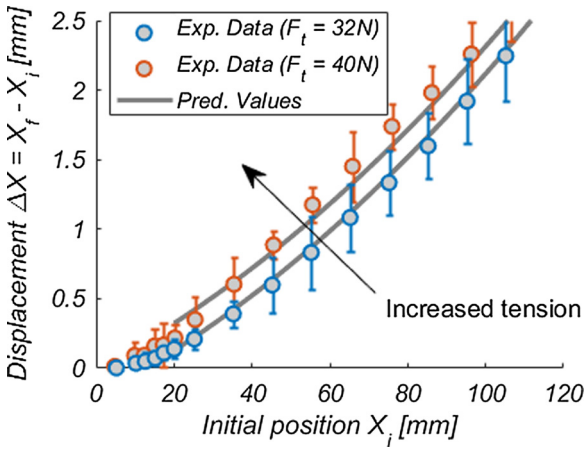

Fig. 11. Experimentally determined deformation of foils during UAM under different levels of tensioning force.

the reduction of the mean layer thickness was independent of the tensioning force (approx. 11.4% measured using the surface profiling system), and the average roughness of the top surface (R_a) of the prepared samples was reduced from 2.96 μm for the low level of the tensioning force to 2.72 μm for the high level.

The important role of the tensioning force in the deformation of the foils during the welding step of the UAM process is one of the key findings of this study. This parameter has often been overlooked in previous studies: most past researchers did not report the level of tension used in their experimentation and it was only implied that sufficient tension was applied to inhibit the movement of the foils during welding. An alternative approach to inhibit movement of the foils during UAM was demonstrated by Schick et al. [34]. In their work, the welding pass was preceded by a tacking pass using lower values for the main UAM processing parameters. This method is considered a standard industrial practice during UAM processing. It should be noted that the elongation of the foil was expected to be lower when lower levels of amplitude and normal force are used, but it was not possible to predict the deformation of the foil during the second pass with the available data. Even though further experimentation is necessary, this investigative analysis highlighted the importance of the tension force in the deformation of the foil.

3.3. Stage 3: the deformation of pre-machined features with variable length and width

The deformation of the width and length of pre-machined features was examined in detail in the third experimental stage for dimensions that are most common for electronic components (i.e. up to 16.8 mm for the length and 7.2 mm for the width, as seen in the catalogues of Texas Instruments [35]. Foils with pre-machined features were prepared, welded and measured in an identical fashion as in Section 3.2. The deformation of the width and length of the features were calculated from the experimentally measured data, as in $\Delta W = |W_f - W_i|$ (the width of the features was decreased after welding) and $\Delta L = L_f - L_i$ (see Fig. 5). A 2nd order linear regression model was fitted on the collected data of lengthwise and widthwise deformation (see Appendix Eqs. (A.6) and (A.7) respectively). The experimental data and the fitted models are presented in Fig. 12. An examination of the response surfaces reveals that the deformation of both the length and width of the pre-machined features was higher for features with a larger initial width (W_i). This was in good agreement with the results of Section 3.2. Notably, the mean width reduction for the examined experimental window was approx. 3.5%, which was considerably higher than the width increase of the foil during welding (i.e. approx. 1% as measured in Section 3.2). Moreover, the error span was not included in this figure

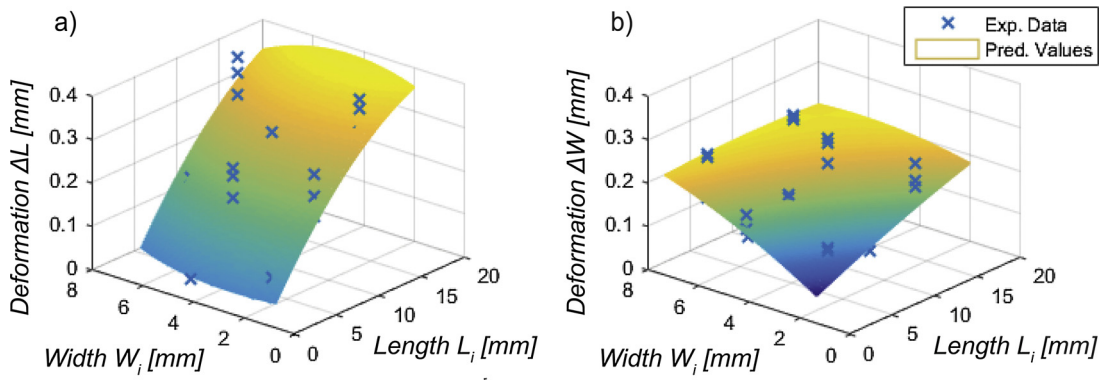

Fig. 12. Experimentally determined response surfaces and experimental data for the (a) lengthwise and (b) widthwise deformation of the pre-machined featured during UAM.

to improve the visualization of the data. In all cases, the deviation from the predicted value was less than 90 μm.

The dimensional tolerance for the width of the features was determined using the topology data collected during the CMM measurements: the surface straightness of the parallel edges (i.e. the machining error) was measured to be approx. $e_{edge} = 0.128$ mm. From the propagation of uncertainty, the dimensional error of the width was calculated as $e_{width} = \sqrt{2} \cdot e_{edge} = 0.181$ and was expressed as a tolerance of ± 0.091 mm. This flat tolerance was preferred over the 95% confidence interval which was used in the estimation of the other errors since the span of the latter was smaller than the value of the former. For the estimation of the dimensional tolerance for the length, the positional error of the edge displacement model of Section 3.2 was used. This was because the value of the tolerance calculated this way was larger than the flat tolerance value calculated from the measured machining error of the front and back edges (0.065 mm and 0.085 mm respectively).

3.4. Single layer validation

A Matlab script was created to predict the final location, dimensions and tolerances of rectangular pre-machined features by combining the experimental regression models described in the previous sections. This script receives as an input the initial dimensions of the pre-machined feature, as well as its initial distance from the start of welding. It is assumed that a force equal to $F_t = 32$ N is used for tensioning. The final location of the front edge was estimated using the enhanced model of Section 3.2 (Eq. (A.5). The equivalent tensioning force was calculated from the width of the pre-machined feature. The final location of the back edge was estimated using the model of Section 3.2 (Eq. (A.3), compensating for the differences in the initial location of the feature from the start of welding when necessary. The length deformation was estimated using the results of the two above steps and the width deformation from the model of Section 3.3. (Eq. (A.7). The associated locational and dimensional errors are estimated from the relevant equations and are combined when necessary using the laws of propagation of uncertainty.

To validate this combined model, three test samples were fabricated. Rectangular slots were machined onto aluminium foils and welded onto a UAM prepared substrate. The location of the features before and after bonding was measured using the CMM system. This resulted in the creation of samples similar to those used for the creation of the model in Section 3.2 (see also Figs. 5 and 6). The nominal, measured and predicted dimensions of these features can be found in Table 2. The initial nominal dimensions were selected, having as a target the fabrication of a cavity for the encapsulation of typical surface mount electronic components.

The measured final location and dimension of all three samples were well within the 95% confidence interval. This suggests that the deformation of pre-machined features can be predicted successfully for a single pre-formed layer bonded via UAM and within the tolerances needed for embedding electronics. The actually measured deviation of the final location and dimensions of the slots was 40%–80% smaller than the predicted error and it was smaller than 50 μm in all cases. In practice such small deviations are unlikely to have a significant impact on the ability to embed electronic components and circuits. Moreover, it is expected that with more precise machining during the forming step, more precise final results can be achieved.

In Table 2 the predicted and actual percentage errors are also presented. These were calculated as the percentage difference between the max./min. predicted by the model value divided by the mean predicted value (in case of the predicted percentage error) and as the percentage difference between the measured and mean predicted value. It can be seen that the predicted error is often overstated, especially for the length. This can be attributed to the relatively large uncertainty associated with the positioning of the foils, which affected the data collection during the creation of the model. The largest actual percentage errors were encountered for the width, which suggests that there is room for improvement. Notably, the absolute error for the width of the features in all cases was less than 50 μm, which is sufficient for most applications.

3.5. Multi-layer form-then-bond structure

To create a multilayer form-then-bond structure, foils with pre-machined features must be stacked layer-by-layer. In this section, the results of the initial investigation towards creating a workflow for using UAM as a form-then-bond process are presented. As an example, a rectangular pocket was manufactured by bonding layer-by-layer six pre-machined foils to accommodate an off-the-shelf SMT resistor (with dimensions 3.10 × 1.65 × 0.55 mm).

For the calculation of the required nominal initial location and dimensions of the pre-machined features, the algorithm of Section 3.4 was expanded. The designed final location and dimensions of the structure were first defined by the user. Then an iterative process was applied until a set of initial nominal values for the location and dimensions of the features on each layer was calculated. This set would produce a structure at the designed location with effective dimensions within a defined margin. A conservative approach was used in the calculations: for each individual layer, the predicted effective final dimensions were defined in such a way so that the resulting feature would have dimensions equal to or larger than the designed dimensions, with a 95% confidence. In other words, the predicted effective final dimensions were defined as the lower limit of the 95% confidence interval to ensure that the electronic component will fit within the fabricated pocket. It was assumed that the deformation of each foil and pre-machined feature were not affected by the previous layers, as the

Table 2
Summary of results of the single-layer validation runs of foils with pre-machined features.

Sample 1							
Initial Nominal Location & Dimensions		$X_{i,nom}$= 21 mm, $L_{i,nom}$= 4.3 mm, $W_{i,nom}$ = 2.8 mm					
Measured Init. Location & Dimensions		Measured Final Location & Dimensions		Pred. Final Location & Dimensions ($\mu \pm 2\sigma$)		Pred. percentage error	Actual percentage error
X_i [mm]	21.013	X_f [mm]	21.105	$X_{f,pred}$ [mm]	21.147 ± 0.109	0.52%	0.20%
L_i [mm]	4.295	L_f [mm]	4.356	$L_{f,pred}$ [mm]	4.361 ± 0.257	5.89%	0.11%
W_i [mm]	2.804	W_f [mm]	2.669	$W_{f,pred}$ [mm]	2.719 ± 0.091	3.35%	1.87%
Sample 2							
Initial Nominal Location & Dimensions		$X_{i,nom}$= 35 mm, $L_{i,nom}$= 4.1 mm, $W_{i,nom}$ = 2.5 mm					
Measured Init. Location & Dimensions		Measured Final Location & Dimensions		Pred. Final Location & Dimensions (μ ± 2σ)		Pred. percentage error	Actual percentage error
X_i [mm]	34.946	X_f [mm]	35.496	$X_{f,pred}$ [mm]	35.450 ± 0.127	0.36%	0.13%
L_i [mm]	4.148	L_f [mm]	4.220	$L_{f,pred}$ [mm]	4.212 ± 0.273	6.48%	0.19%
W_i [mm]	2.456	W_f [mm]	2.387	$W_{f,pred}$ [mm]	2.387 ± 0.091	3.81%	< 0.01%
Sample 3							
Initial Nominal Location & Dimensions		$X_{i,nom}$= 25 mm, $L_{i,nom}$= 4.1 mm, $W_{i,nom}$ = 2.5 mm					
Measured Initial Location & Dimensions		Measured Final Location & Dimensions		Predicted Final Location & Dimensions ($\mu \pm 2\sigma$)		Pred. percentage error	Actual percentage error
X_i [mm]	25.003	X_f [mm]	25.378	$X_{f,pred}$ [mm]	25.308 ± 0.114	0.45%	0.28%
L_i [mm]	4.106	L_f [mm]	4.192	$L_{f,pred}$ [mm]	4.168 ± 0.255	6.12%	0.57%
W_i [mm]	2.442	W_f [mm]	2.325	$W_{f,pred}$ [mm]	2.375 ± 0.091	3.83%	2.15%

foils were aligned to the substrate. By following this approach, the accumulation of errors was avoided.

Three samples were prepared this way. After six foils with pre-machined features were bonded onto a UAM fabricated substrate, an SMT resistor was placed in the produced cavity and secured in place with cyanoacrylate adhesive. These foils were manually aligned first on top of each other and then on top of the substrate before bonding and three small indentations were created on the stack in an area that would not deformed during UAM bonding to use as a guide for the alignment. The resistor was finally encapsulated under two additional aluminium foils. For this experiment, no additional electrically insulating material was used to isolate the resistor, since it was not within the scope of the study. The relevant CMM measurements were taken at every stage of the build and a sample was cross-sectioned and examined under an optical microscope. The results of the design process and the CMM measurements of a representative sample are presented in Table 3. In Fig. 13, the top view of the sample before encapsulation and the cross-section of the back edge of the structure after encapsulation (i.e. the edge along the length of the feature that exhibited the largest error) are presented.

In all prepared samples, very good positional and dimensional (along the length) accuracy was observed: the centre of the pocket was placed in the designed position with accuracy better than 5% and the effective final length ($L_{f,eff}$, see Fig. 13) was, as expected, larger than the predicted effective length and within the predicted by the model 95% interval ($L_{f,pred}$ = 4.168 ± 0.256). The variation observed in the location of the back edge of the structure can be attributed to user error during the manual alignment of the foils or to errors during the pre-machining step. Also, the electronic components retained their functionality after embedding. A resistor was removed from one of the prepared samples after embedding and there was no statistically significant difference between the measured resistance and the value specified by the manufacturer. Moreover, no obvious damage in the resistor was visible in the cross sectioned sample.

However, the measured effective final width ($W_{f,eff}$, see Fig. 13) was smaller than the predicted effective value by approx. 15%. The reason for this discrepancy was the introduction of user error during the manual placement and alignment of the foils before welding. This is evident by the equal interlayer displacement of the foils on the edge of the formed pocket and the top edge of the foils, as shown in Fig. 13, and it was present in all three prepared samples. The alignment error due to manual placement was not taken into account during the generation of the model and it could not be avoided, even though great care was taken during the fabrication of the samples. Nevertheless, the final

Table 3
Summary of results of the design process and measurements of a representative multi-layer structure.

Designed Final Location & Dimensions		$X_{f,des}$= 27.40 mm, $L_{f,des}$= 3.90 mm, $W_{f,des}$ = 2.25 mm			
Calculated Initial Nominal Location & Dimensions		$X_{i,nom}$= 27.05 mm, $L_{i,nom}$= 4.10 mm, $W_{i,nom}$ = 2.45 mm			
Measured Average Initial Location & Dimensions		Measured Effective Final Location & Dimensions		Predicted Effective Final Location & Dimensions	
$X_{i,ave}$ [mm]	27.056 ± 0.012	$X_{f,eff}$ [mm]	27.420	$X_{f,pred}$ [mm]	27.392 ± 0.062
$L_{i,ave}$ [mm]	4.106 ± 0.032	$L_{f,eff}$ [mm]	3.937	$L_{f,pred}$ [mm]	≥ 3.913
$W_{i,ave}$ [mm]	2.442 ± 0.028	$W_{f,eff}$ [mm]	1.915	$W_{f,pred}$ [mm]	≥ 2.285

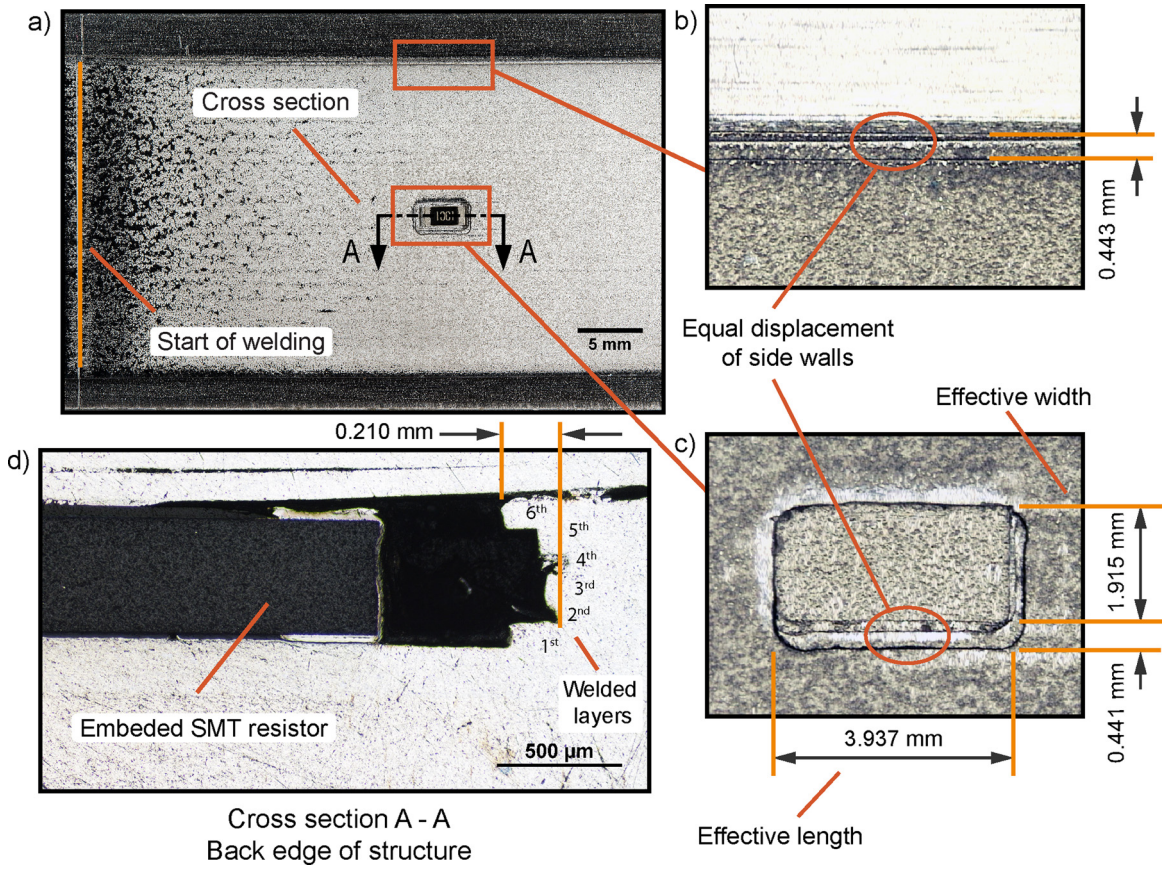

Fig. 13. A representative multi-layer structure. (a) Top view before encapsulation. (b) Close up of the top edge of the bonded foils. (c) Close up of the fabricated structure. (d) Cross section of the back edge of the structure after encapsulation.

Table 4
Final width measurements of each layer of the representative multi-layer structure.

Layer	Measured Final Width (W_f) [mm]
1st	2.339
2nd	2.361
3rd	2.379
4th	2.397
5th	2.388
6th	2.450
Predicted Width:	$W_{f,pred} = 2.375 \pm 0.091$

width of each individual layer after welding was measured by cross-sectioning the sample depicted in Fig. 13 along the width and by examining it under an optical microscope. The results lay well within the values predicted by the model, as shown in Table 4.

Notably, the machine setup was intentionally kept unaltered, in order to evaluate the limitations of the current setup and provide guidance for future improvements. A limitation of all form-then-bond technologies is the need for a precision alignment system, as discussed by Gibson et al. [18] in their review of the sheet lamination technologies. The results of this study indicate that future implementations of the form-then-bond approach in UAM will require the design of a mechanism that will allow the precise placement of the pre-formed foils in the XY plane and also relative to the sonotrode. The development of such a mechanism was outside the scope of this initial investigation to understand the deformation characteristics during the UAM process. However, despite the alignment error, we were able to position and encapsulate one of the smallest SMT devices commonly available with an accuracy of ± 60 µm which is comparable to the resolution obtained for printed interconnects. This shows the feasibility of using form-then-bond as a method for integrating electronics in metal components.

4. Conclusions

In this investigation, the potential use of UAM with the form-then-bond manufacturing approach was examined and confirmed. The elongation characteristics of 100 µm thick Al 3003-H18 foils with and without pre-machined features during the ultrasonic welding step of the UAM process were studied closely and quantified for a set of processing parameters. It was shown that the elongation of the foil and the deformation of the pre-machined features were repeatable and that they follow a 2nd order polynomial law as a function of the distance. Also, it was found that the tensioning force during UAM bonding is of fundamental importance for both the elongation of the foil and the deformation of the pre-machined features. The gathered experimental data was used to create a model for the prediction of the final location, dimensions and associated tolerances of rectangular features. The validation experiments proved that it is possible to successfully use UAM with the form-then-bond approach. The position and dimensions of the fabricated multi-layer structures along the direction of welding were predicted within an accuracy of 5% and 7% respectively. The predictive power of the model increases for structures with larger dimensions because the effect of the machining and alignment errors becomes less prominent. Nevertheless, the developed model should be mainly interpreted as a proof of concept and as a guide for the future development of UAM as a form-then-bond process. Future work must focus on the implementation of a mechanised tensioning system for the precise placement and alignment of the foils prior to UAM bonding. It is expected that the presence of such a system will greatly increase the accuracy of the results and will enable the fabrication of metal

components with embedded 3D electronic circuitry.

Future work should also focus on expanding the created regression model using alternative materials, process parameters and UAM machine setups. This could be accomplished following a similar methodology as that used for the inclusion of the tensioning force. The amplitude, force and speed are expected to introduce an additional – possibly linear - parameter to the model. The temperature has been reported in the literature to affect the material in a simillar way as the amplitude [36]. The metal materials used in UAM have overall a similar mechanical behaviour, so it is expected that only a few calibration runs are required to adjust the model for this. The thickness of the foil plays a role to the deformational characteristics of the material and should also be included to the model to create a unified predictive tool. By gathering additional data points, a process map could be created. It is not clear though whether the model can be directly transferred to different UAM systems without callibration, but the overall response of the elongation of the foil during UAM bonding is expected to follow simillar patterns.

Conflicts of interest

None.

Acknowledgements

This work was supported by the Engineering and Physical Sciences Research Council, UK via the Centre for Innovative Manufacturing in Additive Manufacturing. We thank Mr Jagpal Singh of the Metrology Laboratory, Wolfson School of Mechanical Electrical and Manufacturing Engineering, Loughborough University, UK for his support.

Appendix A

List of fitted linear regression models and corresponding fitted parameters

Nomenclature:

ΔX: Predicted displacement.

X_i & X_f : Initial (before bonding) and final (after bonding) distance from the start of welding.

ΔL: Predicted deformation of the length of pre-machined features.

L_i & L_f: Initial (before bonding) and final (after bonding) length of pre-machined features.

ΔW: Predicted deformation of the length of pre-machined features.

W_i & W_f: Initial (before bonding) and final (after bonding) width of pre-machined features.

μ_i: Linear regression model for the prediction of the mean response of model (i).

σ_i: Linear regression model for the prediction of the standard deviation of model (i).

$a_{i,j}$: Calculated parameter (j) of model (i).

Model 1: Displacement of marks on foils as a function of the initial distance from the start of welding

$$\Delta X_{foil}(X_i) = X_f - X_i = \mu_1(X_i) \pm 2 \cdot \sigma_1(X_i)$$
$$\mu_1(X_i) = a_{1,1} + a_{1,2} \cdot X_i + a_{1,3} \cdot X_i^2$$
$$a_{1,1} = -8.16e-2,\ a_{1,2} = 9.33e-3,\ a_{1,3} = 1.23e-4 \quad \text{(A.1)}$$

$$\sigma_1(X_i) = b_{1,1} + b_{1,2} \cdot X_i$$
$$b_{1,1} = 4.65e-3,\ b_{1,2} = 1.53e-3 \quad \text{(A.2)}$$

Model 2: Displacement edges of pre-machined features as a function of the initial distance from the start of welding

$$\Delta X_{edges}(X_i) = X_f - X_i = \mu_2(X_i) \pm 2 \cdot \sigma_2(X_i)$$
$$\mu_2(X_i) = a_{2,1} + a_{2,2} \cdot X_i + a_{2,3} \cdot X_i^2$$
$$a_{2,1} = -7.91e-2,\ a_{2,2} = 1.74e-2,\ a_{2,3} = 4.55e-5 \quad \text{(A.3)}$$

$$\sigma_2(X_i) = b_{2,1} + b_{2,2} \cdot X_i$$
$$b_{2,1} = -3.92e-2,\ b_{2,2} = 4.17e-3 \quad \text{(A.4)}$$

Model 3: Displacement of marks on foils as a function of the initial distance from the start of welding and the tensioning force

$$\Delta X_{foil,tension}(X_i) = X_f - X_i = \mu_3(X_i, F_t) \pm 2 \cdot \sigma_3(X_i, F_t)$$
$$\mu_3(X_i, F_t) = a_{3,1} + a_{3,2} \cdot X_i + a_{3,3} \cdot X_i^2 + a_{3,4} \cdot F_t$$
$$a_{3,1} = -1.30,\ a_{3,2} = 1.47e-2,\ a_{3,3} = 8.52e-5,\ a_{3,4} = 1.96e-3 \quad \text{(A.5)}$$

$$\sigma_3(X_i, F_t) = b_{3,1} + b_{3,2} \cdot X_i + b_{3,4} \cdot F_t$$
$$b_{3,1} = 3.49e-2,\ b_{3,2} = 1.20e-3,\ b_{3,3} = -2.10e-5 \quad \text{(A.6)}$$

Model 4: Lengthwise deformation of pre-machined features as a function of their initial length and initial width

$$\Delta L(L_i, W_i) = L_f - L_i = a_{4,1} + a_{4,2} \cdot L_i + a_{4,3} \cdot L_i^2 + a_{4,4} \cdot W_i + a_{4,5} \cdot W_i^2 + a_{4,6} \cdot L_i \cdot W_i$$
$$a_{4,1} = -2.06e-1,\ a_{4,2} = 2.68e-2,\ a_{4,3} = 3.28e-5,\ a_{4,4} = 5.95e-2,\ a_{4,5} = -7.37e-3,\ a_{4,5} = 4.71e-4 \quad \text{(A.7)}$$

Model 5: Width deformation of pre-machined features as a function of their initial length and initial width

$$\Delta W(L_i, W_i) = |W_f - W_i| = a_{5,1} + a_{5,2} \cdot L_i + a_{5,3} \cdot L_i^2 + a_{5,4} \cdot W_i + a_{5,5} \cdot W_i^2 + a_{5,6} \cdot L_i \cdot W_i$$
$$a_{4,1} = -7.67e-2,\ a_{4,2} = 1.04e-2,\ a_{4,3} = 6.67e-5,\ a_{4,4} = 5.16e-2,\ a_{4,5} = -2.11e-3,\ a_{4,5} = -1.32e-3 \quad \text{(A.8)}$$

References

[1] White DR. Ultrasonic consolidation of aluminium tooling. Adv Mater Process 2003;161:64–5.
[2] Kong CY, Soar RC, Dickens PM. Optimum process parameters for ultrasonic consolidation of 3003 aluminium. J Mater Process Technol 2004;146:181–7. http://dx.doi.org/10.1016/j.jmatprotec.2003.10.016.
[3] Hopkins CD, Wolcott PJ, Dapino MJ, Truog aG, Babu SS, Fernandez Sa. Optimizing ultrasonic additive manufactured Al 3003 properties with statistical modeling. J Eng Mater Technol 2012;134(11004). http://dx.doi.org/10.1115/1.4005269.
[4] Wolcott PJ, Hehr A, Dapino MJ. Optimized welding parameters for Al 6061 ultrasonic additive manufactured structures. J Mater Res 2014;29:2055–65. http://dx.doi.org/10.1557/jmr.2014.139.
[5] Kelly GS, Just MS, Advani SG, Gillespie JW. Energy and bond strength development during ultrasonic consolidation. J Mater Process Technol 2014;214:1665–72. http://dx.doi.org/10.1016/j.jmatprotec.2014.03.010.
[6] Schick D, Babu SS, Foster DR, Dapino M, Short M, Lippold JC, et al. Transient thermal response in ultrasonic additive manufacturing of aluminum 3003. Rapid Prototyp J 2011;17:369–79. http://dx.doi.org/10.1108/13552541111156496.
[7] Sriraman MR, Gonser M, Foster D, Fujii HT, Babu SS, Bloss M. Thermal Transients during processing of 3003 Al-H18 Multilayer build by very high-power ultrasonic additive manufacturing. Metall Mater Trans B 2011;43:133–44. http://dx.doi.org/10.1007/s11663-011-9590-6.
[8] Kong CY, Soar RC, Dickens PM. A model for weld strength in ultrasonically consolidated components. Proc Inst Mech Eng Part C J Mech Eng Sci 2005;219:83–91. http://dx.doi.org/10.1243/095440605X8315.
[9] Yang Y, Janaki Ram GD, Stucker BE. Bond formation and fiber embedment during ultrasonic consolidation. J Mater Process Technol 2009;209:4915–24. http://dx.doi.org/10.1016/j.jmatprotec.2009.01.014.
[10] Li J, Monaghan T, Masurtschak S, Bournias-Varotsis A, Friel RJ, Harris RA. Exploring the mechanical strength of additively manufactured metal structures with embedded electrical materials. Mater Sci Eng A 2015;639:474–81. http://dx.doi.org/10.1016/j.msea.2015.05.019.
[11] Siggard EJ, Madhusoodananb AS, Stucker B, Eames B. Structurally embedded electrical systems using ultrasonic consolidation (UC) Austin. Proc. 17th annu. solid free. fabr. symp. 2006:70–83.
[12] Robinson CJ, Stucker B, Lopes AJ, Wicker R, Palmer JA. Integration of direct-write (DW) and ultrasonic consolidation (UC) technologies to create advanced structures with embedded electrical circuitry Austin, Texas, USA. 17th solid free. fabr. symp. 2006:60–9.
[13] Kong CY, Soar R. Method for embedding optical fibers in an aluminum matrix by ultrasonic consolidation. Appl Opt 2005;44:6325. http://dx.doi.org/10.1364/AO.44.006325.
[14] Monaghan T, Capel AJ, Christie SD, Harris RA, Friel RJ. Solid-state additive manufacturing for metallized optical fiber integration. Compos Part A Appl Sci Manuf 2015;76:181–93. http://dx.doi.org/10.1016/j.compositesa.2015.05.032.
[15] Mou C, Saffari P, Li D, Zhou K, Zhang L, Soar R, et al. Smart structure sensors based on embedded fibre Bragg grating arrays in aluminium alloy matrix by ultrasonic consolidation. Meas Sci Technol 2009;20(34013). http://dx.doi.org/10.1088/0957-0233/20/3/034013.
[16] Friel RJ, Harris RA. A nanometre-scale fibre-to-matrix interface characterization of an ultrasonically consolidated metal matrix composite. Proc Inst Mech Eng Part L J Mater Des Appl 2010;224:31–40. http://dx.doi.org/10.1243/14644207JMDA268.
[17] Hahnlen R, Dapino MJ. NiTi–Al interface strength in ultrasonic additive manufacturing composites. Compos Part B Eng 2014;59:101–8. http://dx.doi.org/10.1016/j.compositesb.2013.10.024.
[18] Gibson I, Rosen DW, Stucker B. Sheet lamination processes. Addit. manuf. technol.. Boston, MA: Springer US; 2010. p. 223–52.
[19] Cawley JD, Heuer AH, Newman WS, Mathewson BB. Computer-aided manufacturing of laminated engineering materials. Am Ceram Soc Bull 1996;75:75–9.
[20] Thabourey J, Barlier C, Bilteryst F, Lazard M, Batoz J-L. Stratoconception contribution for rapid tooling in die casting: from the design to experiments. Adv Prod Eng Manag 2010;5:121–33.
[21] Bournias-Varotsis A, Friel RJ, Harris RA, Engstrom D. Selectively anodised aluminium foils as an insulating layer for embedding electronic circuitry in a metal matrix via ultrasonic additive manufacturing Austin, TX. Proc. 26th annu. int. SFF symp. 2016:2260–70.
[22] Dumstorff G, Paul S, Lang W. integration without disruption: the basic challenge of sensor integration. IEEE Sens J 2014;14:2102–11. http://dx.doi.org/10.1109/JSEN.2013.2294626.
[23] Swank ML, Stucker BE. Investigation of support materials for use in ultrasonic consolidation. Solid free. fabr. symp.. 2009. p. 231–56.
[24] Kong CY, Soar RC, Dickens PM. Characterisation of aluminium alloy 6061 for the ultrasonic consolidation process. Mater Sci Eng A 2003;363:99–106. http://dx.doi.org/10.1016/S0921-5093(03)00590-2.
[25] The American Society of Mechanical Engineers. Dimensioning and tolerancing (Y14.5 – 2009). ASME; 2009.
[26] Doehlert DH. Uniform shell designs. J R Stat Soc Ser C (Appl Stat) 1970;19(9). http://dx.doi.org/10.2307/2346327.
[27] Ferreira SLC, Bruns RE, da Silva EGP, Dos Santos WNL, Quintella CM, David JM, et al. Statistical designs and response surface techniques for the optimization of chromatographic systems. J Chromatogr A 2007;1158:2–14. http://dx.doi.org/10.1016/j.chroma.2007.03.051.
[28] Pilkey WD, Pilkey Deborah F, Pilkey DF, Pilkey Deborah F. Peterson's stress concentration factors. 3rd ed. Hoboken, NJ, USA: John Wiley & Sons, Inc.; 2007. http://dx.doi.org/10.1002/9780470211106.
[29] Slocum AH. Precision machine design. Society of Manufacturing Engineers; 1992. ISBN: 978-0872634923.
[30] Friel RJ, Johnson KE, Dickens PM, Harris RA. The effect of interface topography for ultrasonic consolidation of aluminium. Mater Sci Eng A 2010;527:4474–83. http://dx.doi.org/10.1016/j.msea.2010.03.094.
[31] Kulakov M, Rack HJ. Surface damage during ultrasonic consolidation of 3003-H18 aluminum. Rapid Prototyp J 2010;16:12–9. http://dx.doi.org/10.1108/13552541011011677.
[32] (Sam) Zhang C, Deceuster A, Li L. A method for bond strength evaluation for laminated structures with application to ultrasonic consolidation. J Mater Eng Perform 2009;18:1124–32. http://dx.doi.org/10.1007/s11665-008-9342-1.
[33] Mielnik EM. Metalworking science and engineering. McGraw-Hill Professional; 1991. ISBN: 978-0070419049.
[34] Schick DE, Hahnlen RM, Dehoff R, Collins P, Babu SS, Dapino MJ, et al. Microstructural characterization of bonding interfaces in Aluminum 3003 blocks fabricated by ultrasonic additive manufacturing. Weld J 2010;89:105–15.
[35] Instruments Texas. Online catalogue. 2017https://www.ti.com/.
[36] Kelly GS, Advani SG, Gillespie JW, Bogetti TA. A model to characterize acoustic softening during ultrasonic consolidation. J Mater Process Technol 2013;213:1835–45. http://dx.doi.org/10.1016/j.jmatprotec.2013.05.008.
[37] Bournias-Varotsis A, Wang S, Hutt D, Engstrøm DS. The Effect of Ultrasonic Additive Manufacturing on Integrated Printed Electronic Conductors. Electron Mater Lett 2018:1–13. http://dx.doi.org/10.1007/s13391-018-0053-y.

Alkaios Bournias-Varotsis has been a post-graduate PhD researcher in Additive Manufacturing at Loughborough University since 2014. His research focuses on the embedding of printed electronics and other electronic circuitry into a metal matrix via ultrasonic additive manufacturing. He graduated with honours from the National Technical University of Athens, receiving a diploma in Mechanical Engineering in 2013.

Dr Ross J. Friel has been a Research Engineer at the MAX IV Laboratory, Lund University, Sweden since 2016, working on the applications of advanced manufacturing technologies to cutting-edge scientific areas such as serial x-ray crystallography of macromolecules and in-situ time-resolved biological sample analysis. Prior to this, he was a Lecturer in Additive Manufacturing at Loughborough University where he worked on many areas of additive and hybrid manufacturing such as in-situ resource utilisation using laser melting, smart metal composites and microfluidic reaction and monitoring devices. Dr Friel was awarded his PhD from Loughborough University, UK in 2011.

Professor Russell Harris, University of Leeds, has been researching manufacturing processes since 1997, primarily in academia, but also with significant links to industry. He has been recognised by the award of three annual IMechE prizes for his research spanning different manufacturing processes and different materials and by the award of the Queen's Anniversary Prize for High-Value Manufacturing in 2013. His work has been funded by the EPSRC, EU, and the Department of Health, alongside industry funding. He has over 100 research papers in manufacturing.

Dr Daniel S. Engstrom has been a lecturer in Additive Manufacturing at Loughborough University since 2015, working on 3D printed electronics, ceramics, metals and nano- and micro-scale additive manufacturing technologies. Prior to this, he was a research associate at the University of Oxford, Imperial College London and UCL working on nanoscale additive manufacturing and nano-manufacturing of point-of-care-devices. Dr Engstrom was awarded a PhD from the Technical University of Denmark in 2011 on MEMS integration with carbon nanotubes in collaboration with the University of Cambridge. He also holds an M.Sc and B.Sc in Applied Physics from the Technical University of Denmark.